https://doi.org/10.48048/tis.2022.4636

Reusability of Nano-Fe_3O_4/Polyvinylidene Difluoride Membrane for Palm Oil Mill Effluent Treatment

Mieowkee Chan[*] and Chiasiang Ooi

Centre for Water Research, Faculty of Engineering, Built Environment and Information Technology, SEGi University, 47810 Petaling Jaya, Selangor, Malaysia

([*]Corresponding author's e-mail: mkchan@segi.edu.my)

Received: 22 February 2021, Revised: 3 June 2021, Accepted: 3 July 2021

Abstract

Membrane reusability determines the economic sustainability of separation process. However, the reusability of membrane was deduced by the antifouling properties, while the actual reuse performance of membrane using palm oil mill effluent (POME) is rarely reported. This study investigates the reusability of nano-Fe_3O_4/PVDF (PVDF1) membrane for POME treatment. The chemical oxygen demand (COD), total suspended solid (TSS) of permeate, molecular weight cut off (MWCO), pure water flux (PWF) and contact angle (CA) of membranes were also determined. Result showed that the neat membrane (PVDF0) and PVDF1 exhibited ~77°, ~342 L/(m^2.h) and ~70°, 278 L/(m^2.h) for CA and PWF, respectively, due to the small MWCO in PVDF1. The POME flux was maintained at ~16 L/(m^2.h) in 5 cycles of filtration process. The COD rejection was higher for PVDF 1 compared to PVDF0, and PVDF1 showed consistent ~58 % COD and ~98 % TSS removal in all the cycles. The good performance of PVDF1 due to the presence of nano-Fe_3O_4, improved the membrane hydrophilicity and tailored the membrane pore size for POME treatment.

Keywords: POME, Nano-Fe_3O_4/PVDF membrane, Reusability, hydrophilicity, TSS

Introduction

Agriculture is the third contributor to the gross domestic product in Malaysia after the servicing and manufacturing sectors [1]. According to the work published by Malaysian Agricultural Research and Development Institute (MARDI), oil palm occupied the largest land use, which was 5,672 thousand hectare in 2020 and followed by rubber which was 1197.6 thousand hectare [2]. The export of palm oil and the related products contributed approximately US$1 billion [3]. Despite its contribution to the economy, the oil palm processing pollutes a large volume of water. Water is used as the feed for boiler and as the diluent in the refining process to enhance the oil separation [4]. It was estimated that 0.114 m^3 of water/tonne fresh fruit bunches was used in the purification process. Water is also used to sterilise the palm fruit bunch [5]. The polluted water is generally known as palm oil mill effluent (POME) and it consists of 51,000 mg/L of chemical oxygen demand (COD), 25,000 mg/L biological oxygen demand (BOD) and 18,000 mg/L of total suspended solid (TSS) at pH 9.0 [6]. Besides, other minerals such as potassium, calcium and phosphorus are also present in POME. According to Department of Environment (DOE), the discharge limit for BOD3 and TSS are 100 and 400 mg/L, respectively with pH within 5.0 - 9.0 [6,7]. COD shall be maintained at non-detectable limit. Open ponding system which consists of cooling and mixing, anaerobic, facultative and aerobic ponds, is widely adopted to treat POME in order to minimise the undesirable impact on the environment [6]. To date, the need to comply with the latest stringent DOE discharge limit as well as the introduction of 0 effluent discharge concept, attempts have been made to incorporate membrane technology to enhance the quality of effluent. Study conducted by Loh *et al*. [8] showed that the effluent consisted of approximately 700 mg/L of COD, < 20 mg/L of BOD3 and 0.8 NTU after ultrafitration treatment. TSS was not detectable in the effluent. In the study conducted by Hadi *et al.* [9] the BOD reading was reduced from 50 mg/L to < 10 mg/L in the presence of polishing plant, which consisted of a bioreactor and polyvinylidene difluoride (PVDF) membrane.

PVDF is the widely used membrane forming material due to its high mechanical strength and excellent chemical and thermal resistance properties. However, PVDF membrane is prone to foul due to its native hydrophobic property. Fouling reduces the flux, separation performance as well as the life span

of the membrane which leads to high operational cost. Numerous attempts have been made to improve the antifouling property of PVDF membrane by alternating the surface properties of membranes. Subramaniam *et al.* [10] added 0.5 wt% of titanate nano tubes to the PVDF membrane and it reduced the contact angle of neat membrane from 75.18 to 64.91 °. The membrane exhibited > 90 % flux recovery ratio after 5 cycles of aerobically-treated palm oil mill effluent (AT-POME) filtration. Similar to the work done by Ho *et al.* [11], where oxidized multi-walled carbon nanotubes (OMWCNT) enhanced hydrophilicity of neat PVDF membrane from 73.33 to 71.77 °. The surface charge of the membranes was reported as −22.2 and −12.8 mV for PVDF/OMWCNT membrane and neat membrane, respectively. This surface properties improved the antifouling of the membrane where the normalised flux was 0.26 for PVDF/OMWCNT membrane while 0.12 was recorded for the neat membrane.

Table 1 The contact angle and fouling data of nano-Fe_3O_4 impregnated membrane.

Polymer	Method	Antifouling performance	Application	References
PES (NF)	Nano-Fe_3O_4/PVP was blended into the polymer matrix	Contact angle: 55 ° Feed: 200 ppm BSA solution FRR: 89.5 %	Desalination	[49]
PES (NF)	Nano-Fe_3O_4/O-carboxymethyl chitosan was blended into the polymer matrix	Contact angle: 53.2 ° Feed: powder milk solution FRR: 91.7 %	Dye removal	[16]
PVDF (UF)	Nano-Fe_3O_4/O-carboxymethyl chitosan was blended into the polymer matrix	Contact angle: 53.1 ° Feed: Activated sludge suspension FRR: 95.7 %; R_t : ~75 %	Membrane bioreactor use	[50]
PES (UF)	Percarboxylic acid functionalised silica coated nano-Fe_3O_4 was blended into the polymer matrix	Contact angle: 51.2 ° Feed: 200 ppm BSA solution FRR: 91.7 % R_t : ~35 %	Dye removal	[51]
PVDF (UF)	TiO_2 coated nano-Fe_3O_4 was blended into the polymer matrix	Contact angle: ~55 ° Feed: 20 ppm humic acid FRR: 91.10 %,R_t: 69.59 %	-	[52]

R_t : total pollution index

Nano-Fe_3O_4 is hydrophilic, low cost and environmentally safe. Thus, research has been done to impregnate nano-Fe_3O_4 into ultrafiltration (UF) and nanofiltration (NF) membranes to improve the hydrophilicity and antifouling properties of the membranes, as shown in **Table 1**. Generally, nano-Fe_3O_4 incorporated membranes have lower contact angle compared to the neat membranes, which is within 75 to 88 ° for PES and PVDF [12-15]. The nano-Fe_3O_4 impregnated membranes exhibited good flux recovery ratio (FRR), which was approximately 90 % regardless of the composition of the feed. Meanwhile, good separation also observed in these membranes, for example the nano-Fe_3O_4/O-carboxymethyl chitosan PES membranes showed 99 % direct red 16 dye removal [16] while polyaniline/nano-Fe_3O_4/PES membrane removed 80 % of copper [17].

Generally, most of the antifouling experiment reported in the literature, such as FRR and R_t shown in **Table 1** was conducted only once, where the reusability of the membrane for practical application remains unknown. Besides, current research mainly focused on the FRR of membrane to deduce the reusability [18,19]. The actual separation performance of reusing the membrane is rarely reported.

Besides, limited research has been done to find out the performance of nano-Fe_3O_4 in treating POME. This study investigates the reusability of nano-Fe_3O_4/PVDF membrane for POME application. Five cycles of filtration by using POME as feed was conducted to reveal the actual performance of the membrane for real life application. The separation performance of every cycle also reported in terms of COD and TSS removal.

Materials and methods

PVDF (Mw = ~534,000) and polyvinylpyrrolidone K30 (PVP, K30) were supplied by Sigma-Aldrich and Vchem Laboratory Chemicals, respectively. N, N-Dimethylformamide (DMF) with the purity of > 99.8 %, ethanol with 99 % purity and 0.1M ethylenediaminetetraacetic acid (EDTA) were supplied by Fisher Scientific. $FeSO_4.7H_2O$ and Na_2CO_3 were obtained from Merck Germany. All the chemicals were used without further purification.

Biological-treated POME was obtained from the extended aerobic pond at a local mill factory, Teluk Intan, Perak. The collected POME consisted of 992.00 ± 40.18 mg/L of TSS and 2300.73 ± 136.69 mg/L of COD at pH 8.53. The solution was stored at 4 °C to avoid microbial decomposition.

Preparation and characterization of nano-Fe_3O_4

Nano-Fe_3O_4 was synthesised by using 0.05M of EDTA as the chelating agent [20] and 0.75 M Na_2CO_3 as the reducing agent. Na_2CO_3 was added drop-wise to 0.1 M of $FeSO_4$ solution under stirring speed of 300 rpm. The black precipitate nano-Fe_3O_4 was immersed in 1.0 M of sodium carbonate to complete the reduction process. The nano-Fe_3O_4 was rinsed 3 times using ethanol and stored in ethanol before use.

The morphology and the size of iron oxide nanoparticle was observed by using field emission scanning electron microscopy (FESEM, ZEISS SUPRA 35VP). The sample was coated with a thin layer of gold under vacuum to avoid the charge effect on sample. The magnification of the images was captured at 10 and 70 kX to clearly capture the size and shape of nano-Fe_3O_4.

X-ray diffraction model PANalytical, EMPYREAN was used to analyze the crystal structure of nano-Fe_3O_4. The sample was exposed to CuKα radiation at the wavelength of 1.54060 Å (0.15406 nm) in 2θ range of 10 - 70 °. The size of nano-Fe_3O_4 can be estimated using the Scherrer's formula Eq. (1) [21,22];

$$D = \frac{K\lambda}{\beta cos\theta} \quad (1)$$

D is crystalline particle size, K is Scherrer constant, which is 0.9 for nano-Fe_3O_4, λ = X-ray wavelength with CuKα (0.15406 nm), β = full width at half maximum (FWHM) in radian and lastly θ is Bragg angle in radian.

Fabrication and characterisation of nano-Fe3O4/PVDF membrane

Nano-Fe_3O_4/PVDF membranes with varied concentrations of nano-Fe_3O_4 was prepared as per the formulation in **Table 2**. Appropriate amount of nano-Fe_3O_4 was firstly dispersed in DMF in an ultrasonic vibrator for 60 min. 19 wt% of PVDF and 3 wt% of PVP were then added into the nano-Fe_3O_4 – DMF mixture and stirred at 400 rpm for 4 h at 85 °C [23,24]. The bubble-free solution was cast by using the semi-automated casting machine at 7 cm/s [25]. The blade of the semi-automated casting machine was adjusted to cast a film with 200 µm thickness. The casted film was immersed into reverse osmosis (RO) water bath after the film was exposed to the hot air in oven for 9 min at 60 °C. After the dry-wet phase inversion process, the membrane was rinsed and preserved in RO water before use.

Table 2 The dope formulation of nano-Fe_3O_4/PVDF membrane.

Membrane ID	PVDF	PVP	DMF	nano-Fe_3O_4
PVDF0	19	3	78	0.0
PVDF1	19	3	77.9	0.1
PVDF2	19	3	77.8	0.2

The surface and cross-sectional morphologies of the membranes were imaged by using FESEM (ZEISS SUPRA 35VP). The sample was freeze-fractured using liquid nitrogen to obtain a perfect clear cut for the cross-sectional image. The membrane was coated with gold before imaging.

The hydrophilicity of the membrane was determined by the contact angle goniometer (Attention ThetaLite101) with RO water as the liquid. The angle between the 3 µL water droplet and the membrane surface was captured by the attached high-speed camera in the goniometer. Minimum of 10 different spots of the membrane were measured for accuracy and precision purpose.

The functional groups of the fabricated membrane were identified by using Perkin Elmer Spectrum One FT-IR Spectrometer. Minimum of 16 scans were set to every sample within the wavelength from 800 to 4000 cm^{-1}.

The density of the membrane was measured by using gravimetric method. Molecular weight cut off (MWCO) of the membranes were determined from the solutes rejection of 20,000 g/mol polyethylene glycol (PEG), 34,500 g/mol pepsin, 46,000 g/mol egg albumin (EA) and 66,500 g/mol bovine serum albumin (BSA). The experiment was conducted in a 50 mL Milipore dead-end stirrer filtration cell with an effective membrane area of 13.4 cm^2 under the pressurised nitrogen gas of 1 bar. The concentration of PEG was measured by using Dragondorff's Reagent [26] at 510 nm while the concentration of pepsin, EA and BSA were determined at wavelength of 280 nm [27]. The solute rejection (R) was calculated by using Eq. (2), where C_p is the concentration of permeate and C_f is the concentration of the feed.

$$R = \left(1 - \frac{C_p}{C_f}\right) \times 100\ \% \tag{2}$$

The experiment was repeated by using pure water as the feed to determine the pure water flux (PWF). PWF in $L/m^2.h$ was calculated by Eq. (3) below;

$$PWF = \frac{V}{At} \tag{3}$$

where V is volume of the collected permeate (L) over a duration (t) in hour, and A is effective membrane area, m^2.

Reusability study

POME was used as the feed in the Milipore dead-end stirrer filtration cell. Appropriate amount of permeate was collected and the TSS and COD of permeate were measured by HACH DR-3900 with photometric method 8006 and APHA Standard method 8000, respectively. The experiment was repeated for 5 cycles, and the membrane was cleaned by simple backwashing process using RO water before use in the next cycle.

The antifouling properties of the membrane was quantified as the total pollution index (R_t). J_p is the flux of the POME while the J is the PWF calculated from Eq. (3).

$$R_t = \left(1 - \frac{J_p}{J}\right) \times 100 \tag{4}$$

Results and discussion

Properties of nano-Fe_3O_4

The surface morphology of nano-Fe_3O_4 is shown in the FESEM images in **Figure 1**. It is clearly show that the nano-Fe_3O_4 has a spherical shape with the average size ranged from ~24 to ~37 nm, which confirms the formation of nano-sized particle. The images are similar to the nano-Fe_3O_4 produced by Rabel *et al.* [28] and Mahdavi *et al.* [29] where ammonia solution was used as the reducing agents. Comparatively, the use of Na_2CO_3 to produce nano-Fe_3O_4 in this study is a better reducing agent compared to ammonia solution due to low toxicity.

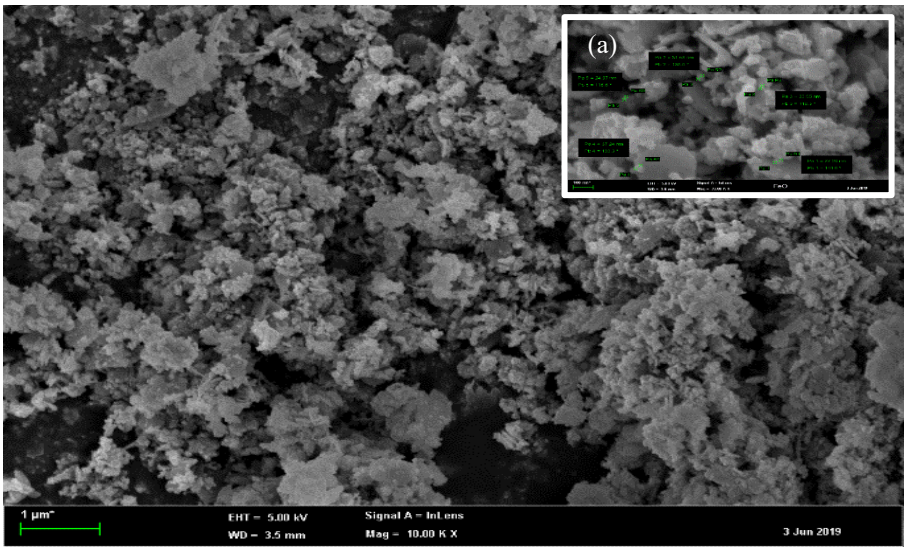

Figure 1 FESEM image of nano-Fe_3O_4 at 10 kX; (a) Particle size at 5 random points was measured: 24.97, 31.68, 23.55, 37.24 and 37.20 nm.

The composition of nano-Fe_3O_4 is confirmed by the XRD spectrum shown in **Figure 2**, where the diffraction peaks are observed at 2θ = 18.5, 30.3, 35.7, 44.9, 53.8, 57.3 and 62.8 °. The peaks are in consistent with the peaks observed in magnetite Fe_3O_4 elements [30,31]. According to Scherer's equation (Eq. (1)), the average size of crystalline particle size is approximately 36 nm at diffraction peak of 35.7 °. The particle size is similar to the size measured from FESEM image in **Figure 1**.

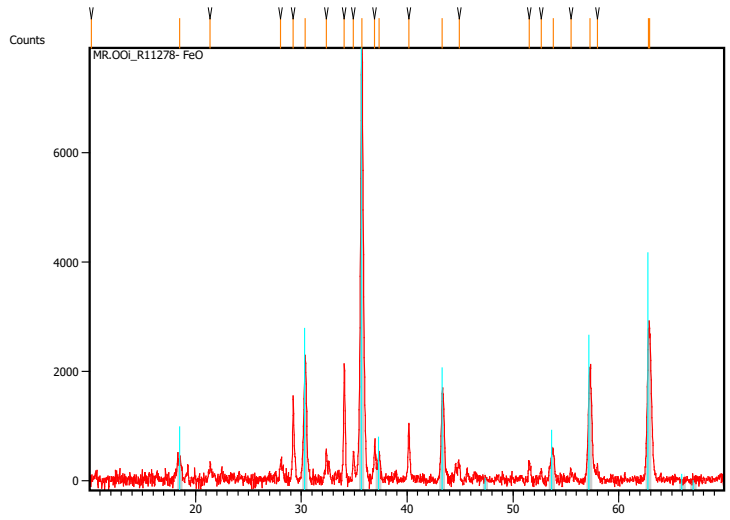

Figure 2 XRD pattern of nano-Fe_3O_4.

Properties of nano-Fe_3O_4/PVDF membranes

FTIR spectra in **Figure 3** show the signature bands of PVDF-PVP membranes, where the bands near to 840, 1073 and 1400 cm^{-1} indicate the vibration of β-PVDF [32]. C=O stretching vibration due to the presence of PVP is observed at ~1660 cm^{-1} [33,34]. The bands at ~1180 and 1277 cm^{-1} show the $–CF_2$ stretching vibration and β phase vibration, respectively [35]. It is notable that the presence of nano-Fe_3O_4 in PVDF1 and PVDF2 did not cause any formation of new bonding or destruction of existing bonding. This finding is in agreement with the works published by Chen *et al.* [33] where the addition of metallic additive to the casting solution did not disrupt the backbone of PVDF-PVP membranes.

Nevertheless, **Figure 3(a)** shows an increment in the intensity of β-PVDF band within the region of 1400 - 800 cm^{-1}. Harstad *et al.* [36] reported the similar finding and suggested that the presence of magnetic particles in PVDF affected the β-PVDF by inducing nucleation in the β phase. It was due to the static electronic interactions between the negatively charged particle and positively charged CH_2 groups. Thus, an increase in the β phase was observed in the FTIR spectrum of Gd_5Si_4/PVDF membrane compared to the neat membrane. This is further supported by the recent work published by Xiong *et al.* [37] where the increase in the intensity of β-PVDF suggested the role of nano-ZnO in enhancing crystallization of β-PVDF. Hence, it is suggested that nano-Fe_3O_4 induces the nucleation in the β-PVDF of PVDF1 membrane and the growth of crystal further enhanced in PVDF2 membrane.

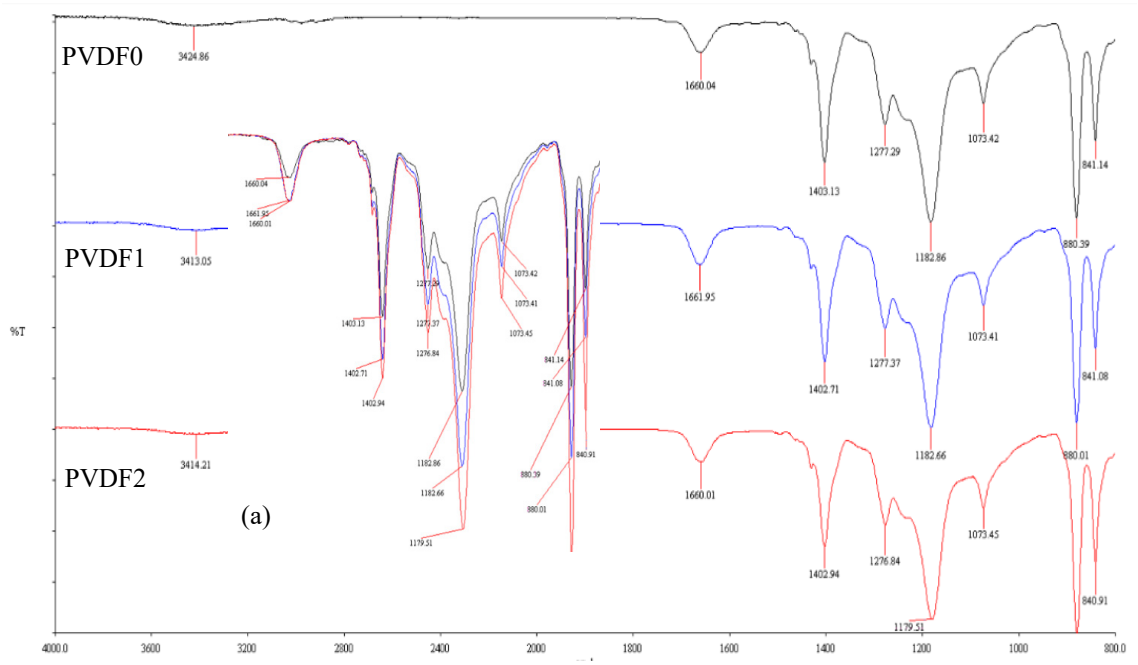

Figure 3 FTIR spectra of nano-Fe_3O_4/PVDF membranes with (a) overlapped image.

Figure 4 illustrates the cross-sectional structure and the surface morphology of nano-Fe_3O_4/PVDF membranes. An asymmetric structure with a thin skin layer and finger-like sublayer is observed in PVDF0 membrane, **Figure 4(a)**. Spherical nodules are found on the surface due to the crystalline structure of PVDF [38] as illustrated in **Figure 4(b)**. The presence of nano-Fe_3O_4 in PVDF1 elongated the finger-like structure in the sublayer due to the enhanced demixing rate during the phase inversion process. The increase in the demixing rate was due to the hydrophilic nature of nano-Fe_3O_4, which caused the exchange of DMF (solvent) and RO water (nonsolvent) easier and thus increased the size of voids, as seen **Figure 4(c)**. This description is supported by the contact angle of PVDF1 membrane, which is approximately ~7 ° lower compared to PVDF0, as shown in **Table 3**. According to Ba-Abbad *et al.* [39], they explained this observation as role of iron oxide in reducing the interface energy of membrane. Hence, the water droplet was easy to spread and attached to the membrane surface. Besides, the hydrophilic nature of nano-Fe_3O_4 also tended to migrate to the water and membrane interface during the phase inversion process.

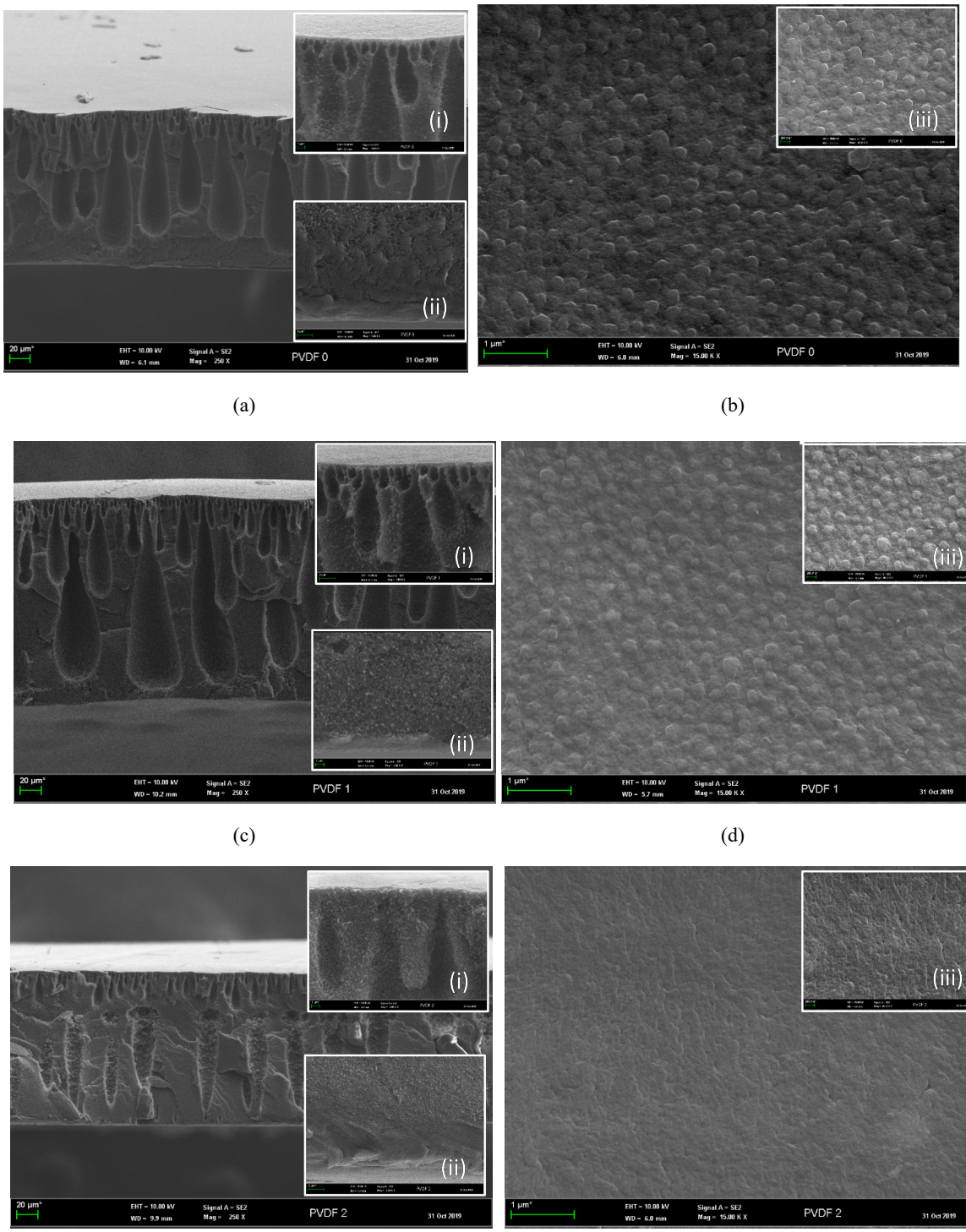

Figure 4 FESEM images of the cross sectional and surface structure of (a) - (b) PVDF0, (c) - (d) PVDF1 and (e) - (f) PVDF2; (i) - (iii) were the magnified (a) - (f) images at 30 kX.

Table 3 Density, contact angle, MWCO and PWF data of nano-Fe_3O_4/PVDF membranes.

Membrane ID	Density (kg/m^3)	Contact angle (°)	MWCO (Da)	PWF (L/(m^2.h))
PVDF0	0.6414	77.126 ± 1.580	44,000	342.43 ± 14.63
PVDF1	0.7930	70.988 ± 2.719	40,000	278.97 ± 25.52
PVDF2	0.8474	74.606 ± 2.042	35,000	97.73 ± 12.04

When the concentration of nano-Fe_3O_4 further increased in PVDF2, it behaved as the heterogeneous nucleating agent, provided interconnections between the crystalline structures and thus produced a smooth surface, as shown in **Figure 4(f)**. This is in agreement with the finding reported by Mago *et al.* [40], where the multiwall carbon nanotubes improved the surface of PVDF membrane by increasing the nucleation process and enabled the crystallization process to proceed to a greater extent. Mago *et al.* [40] emphasized that this process happened at slow demixing rate. In this current study, the demixing rate was slightly delayed in PVDF2 membrane as the viscosity of the casting solution increased due to higher concentration of nano-Fe_3O_4 compared to PVDF1 [41]. This also explains the suppressed figure-like structure and the dense sublayer as shown in **Figure 4(e)**. The density of PVDF2 membrane tabulated in **Table 3** further support this statement where the dense structure contributed to the high density value of PVDF2 membranes.

Notably, the contact angle of PVDF2 is 74.6 °, which is slightly higher compared to PVDF1 even though PVDF2 contains higher amount of nano-Fe_3O_4 than PVDF1, as tabulated in **Table 3**. This may due to the combinatorial effects of porosity, pore size as well as the pure water flux of the membranes [42].

Data in **Table 3** showed that the presence of nano-Fe_3O_4 reduced the pore size and the PWF of the membranes. The MWCO of the membrane was reduced from 44 kDa for PVDF0 to 40 kDa for PVDF1. At the same time, the PWF was reduced from 342.43 to 278.97 L/(m^2.h). PVDF2 exhibited the lowest MWCO at 35 kDa and 97.73 L/(m^2.h). This may due to the presence of nano-Fe_3O_4 in reducing the pore size of the membrane. When the concentration of nano-Fe_3O_4 further increased to 0.2 wt% in PVDF2, the agglomeration of nanoparticles occurred and hence further reduce the MWCO of membrane and reduced the PWF. Similar finding was reported by Tan *et al.* [43] where the reduction in water flux was observed when the ZIO concentration exceeded 1wt% as it caused agglomeration in the membrane matrix. Among the nano-Fe_3O_4/PVDF membranes, PVDF1 exhibited the lowest contact angle with good PWF. Thus, PVDF 1 was selected for the antifouling studies and PVDF0 served as the control.

Reusability study

The data in **Figure 5** shows that the R_t for both PVDF0 and PVDF 1 membranes are similar, which is approximately 95 %. Although the presence of nano-Fe_3O_4 does not contribute significantly to the impact on Rt, but it affects the COD removal. COD reading of the permeate collected from PVDF 1 membrane was lower compared to PVDF0 in the first 3 cycles. It is because of the smaller MWCO of the PVDF1 compared to PVDF2, as shown in **Table 3**. In the 4th and 5th cycle, COD reading for both PVDF0 and PVDF1 is similar. This may be due to the formation of filter cake on the surface of PVDF0 during the filtration process. This developed the resistance to the organic compounds and made it difficult to pass through the membrane. Notably, PVDF1 shows consistent performance in COD removal from all 5 cycles, which is desired for long terms usage.

The bars in **Figure 6** shows that both PVDF0 and PVDF1 membranes exhibited the lowest POME flux in the first cycle. According to **Table 3**, the flux of PVDF1 was ~278 L/(m^{2}h) and it reduced to 14.4 L/(m^{2}h) when POME was used as the feed. This was due to the presence of varied pollutants which were blocked by the membrane, increased the resistance to water flow. Comparatively, PVDF0 experienced a more severe flux reduction from ~342 to ~15.8L/(m^{2}h) when treating POME.

Both PVDF0 and PVDF1 membranes exhibited higher POME flux after the first cycle. This may be due to the backwashing process which had slightly increased the pore size and lead to higher POME flux. This deduction is supported by Akhondi *et al.* [44] where backwashing enlarged the pore size of PVDF membrane. Although the membrane pore size was increased, but the performance of PVDF 1 remain constant in all the 5 cycles of filtration process for both TSS and COD removal as shown in **Figures 5** and **6**. Meanwhile, PVDF0 membrane exhibited similar COD and TSS removal as PVDF 1 after the 4th

cycle of POME treatment. It is assumed that the accumulated foulants on the membrane surface created the resistance to the pollutants. Similar findings were reported by Zheng *et al.* [45] where membrane fouling increased the sulfamethoxalo rejection for forward osmosis membrane.

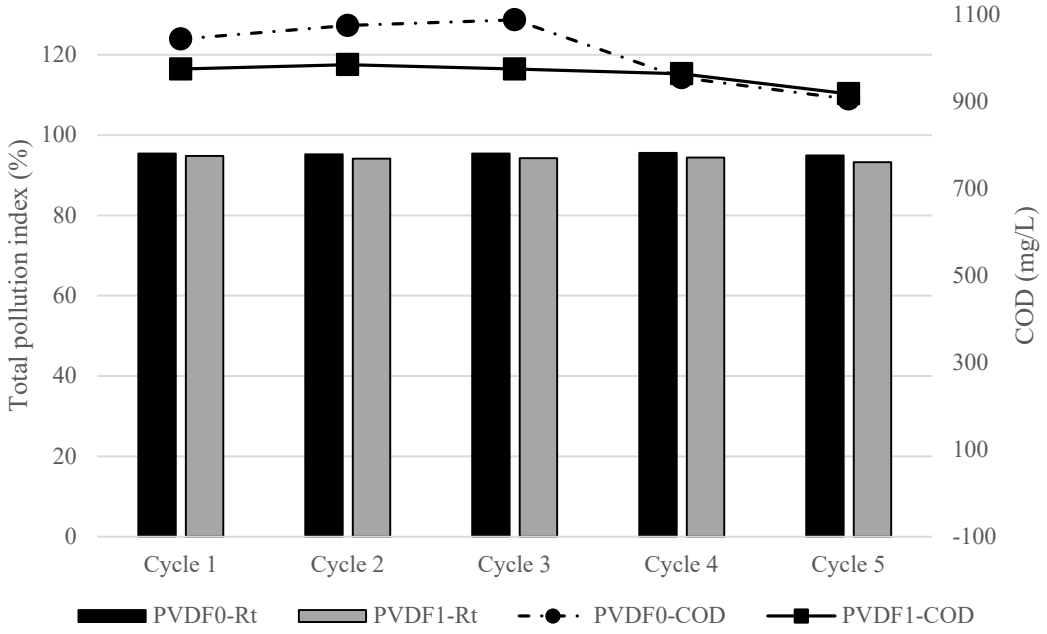

Figure 5 Performance of PVDF0 and PVDF1 membranes in terms of total pollution index and COD.

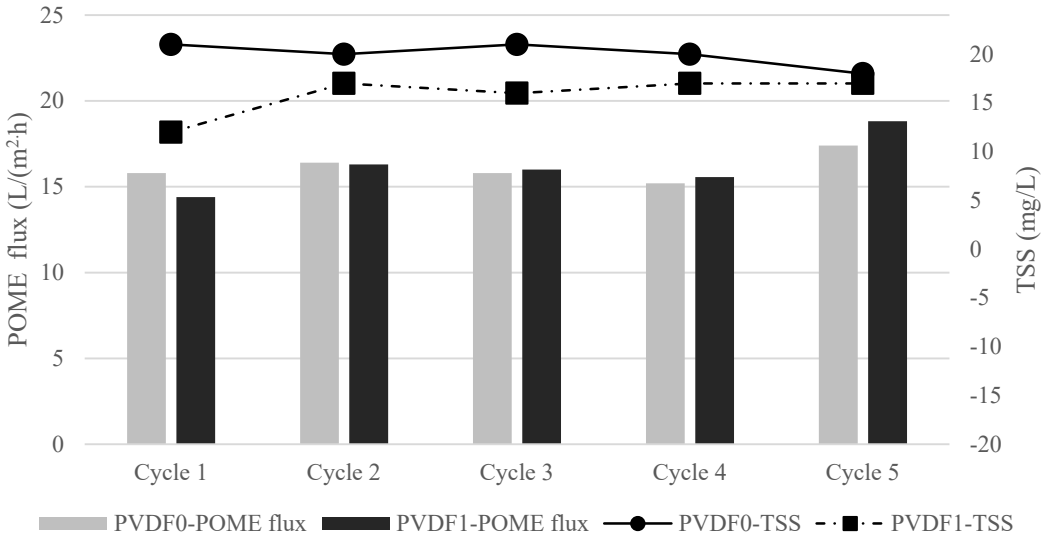

Figure 6 Performance of PVDF0 and PVDF1 membranes in terms of POME flux and TSS.

The performance of PVDF1 is compared with the other UF membranes, which were used for POME treatment, as shown in **Table 4**. The findings showed that most of the UF membranes including PVDF1 were able to remove more than 90 % of TSS. This is because the suspended solids in POME were within the range of 100 - 700 micron [46,47] and UF membranes with the pore size between 0.01 to 0.1 µm are able to block the particles from penetrating through the membrane. Besides, it is notable that the feed

properties governs the performance of the UF membrane. When the feed consisted of high concentration of TSS and COD, for instance in the study done by Anwar et al. [48], the nano-silver coated hydroxyapatite/ polyphenylsulfone membranes removed 91 % of TSS and 97.67 % of COD, but the permeate still did not meet the discharge limit. Thus, pre-treatment process before the membrane separation is crucial in determining the membrane performance. The performance of PVDF1 membrane produced in this study is comparable with the UF membranes reported in the literature. The data also depicts that PVDF1 could be reused at least for 5 cycles with simple backwashing technique using RO water. Additional treatment such as grafting on PVDF1 shall be conducted in the near future to improve the COD removal.

Table 4 Performance of ultrafiltration membranes in treating POME.

Membrane	Properties of Feed	Performance	References
Nano-silver coated hydroxyapatite/ polyphenylsulfone membrane	TSS: 5000 mg/L COD: 4300 mg/L	Concentration of permeate: TSS: 450 mg/L (91.00 % removal) COD: 100 mg/L (97.67 % removal)	[48]
Nano-TiO2/PES-PVP membrane	Not available	TSS removal: 85 %	[53]
PES membrane supplied by Sterlitech	TSS: 3103 mg/L COD: 12,040 mg/L	Concentration of permeate:- TSS: 177 mg/L (94.30 % removal) COD: 619 mg/L (94.86 % removal)	[54]
Graphene oxide/oxidized multi-walled carbon nanotubes – PVDF membrane	TSS: 141.67 mg/L COD: 151 mg/L	TSS removal: 100 % COD removal: 75.5 %	[11]
Nano-Fe_3O_4/PVDF membranes	TSS: 992 mg/L COD: 2300 mg/L	Concentration of permeate:- TSS: 12 mg/L (98.79 % removal) COD: 975 mg/L (57.61 % removal)	This study

Conclusions

The good separation performance of PVDF1 was due to the presence of nano-Fe3O4, which improved the membrane hydrophilicity and tailored the membrane pore size for POME treatment. Consistent permeate flux of ~16 L/(m^2.h), 58 % COD and 98 % TSS removal rate showed that PVDF1 can be reused for 5 cycles filtration process with simple RO backwashing technique.

Acknowledgements

This work was supported by the SEGi University, Malaysia. Special thanks to Syarikat Peladang Dan Perusahaan Minyak Sdn Bhd, Teluk Intan, Perak for supplying the POME samples.

References

[1] Bank Negara Malaysia. *Economic and financial developments in the Malaysian economy in the fourth quarter of 2019*. Bank Negara Malaysia, Kuala Lumpur, Malaysia, 2020.
[2] RA Dardak. *Malaysia's agrofood policy (NAP 2011 - 2020): Performance and new direction*. FFTC Aricultural Policy Platform, Taipei, Taiwan, 2019, p. 1-13.
[3] RA Dardak. *Overview of agriculture trade in Malaysia*. FFTC Aricultural Policy Platform, Taipei, Taiwan, 2019, p. 1-7.

[4] H Sabriyah, D Kospa, KRD Lulofs, C Asdak and SE Rahim. Strategies to reduce water footprint in palm oil production: A case of PTP Mitra Ogan, Baturaja, South Sumatra. *MATEC Web Conf.* 2017; **97**, 01122.

[5] H Kamyab, S Chelliapan, MF Din, S Rezania, T Khademi and A Kumar. *Palm oil mill effluent as an environmental pollutant*. *In*: VY Waisundara (Ed.). Palm oil. IntechOpen, London, 2018, p. 13-28.

[6] NH Zainal, NF Jalani, R Mamat and AA Astimar. A review on the development of palm oil mill effluent (POME) final discharge polishing treatments. *J. Oil Palm Res.* 2017; **29**, 528-40.

[7] YJ Chan and MF Chong. Palm oil mill effluent (POME) treatment - current technologies, biogas capture and challenges. *In*: DCY Foo and MKTA Aziz (Eds.). Green technologies for the oil palm industry. 1st ed. Springer, Singapore, 2019, p. 71-92.

[8] SK Loh, ME Lai, M Ngatiman, WS Lim, YM Choo, Z Zhang and J Salimon. Zero discharge treatment technology of palm oil mill effluent. *J. Oil Palm Res.* 2013; **25**, 273-81.

[9] AH Numan, H Yahaya, N Muzzammil, JN Faizah, WN Abdul and HR Mohamed. Assessment of the effluent polishing plant uisng a ultrafiltration membrane installed at a palm oil mill. *Environ. Protect. Eng.* 2019; **45**, 155-70.

[10] MN Subramaniam, PS Goh, WJ Lau, YH Tan, BC Ng and AF Ismail. Hydrophilic hollow fiber PVDF ultrafiltration membrane incorporated with titanate nanotubes for decolourization of aerobically-treated palm oil mill effluent. *Chem. Eng. J*. 2017; **316**, 101-10.

[11] KC Ho, YH Teow, WL Ang and AW Mohammad. Novel GO/OMWCNTs mixed-matrix membrane with enhanced antifouling property for palm oil mill effluent treatment. *Sep. Purif. Tech.* 2017; **177**, 337-49.

[12] W Wang, L Zhu, B Shan, C Xie, C Liu, F Cui and G Li. Preparation and characterization of SLS-CNT/PES ultrafiltration membrane with antifouling and antibacterial properties. *J. Membr. Sci.* 2018; **548**, 459-69.

[13] Z Low, J Ji, D Blumenstock, Y Chew, D Wolverson and D Mattia. Fouling resistant 2D boron nitride nanosheet - PES nanofiltration membranes. *J. Membr. Sci.* 2018; **563**, 949-56.

[14] Y Jin, D Hu, Y Lin and L Shi. Hydrophilic modification of polyvinylidene fluoride membrane by blending amphiphilic copolymer via thermally induced phase separation. *Polym. Adv. Tech*. 2019; **30**, 110-9.

[15] L Shen, S Feng, J Li, J Chen, F Li, H Lin and G Yu. Surface modification of polyvinylidene fluoride (PVDF) membrane via radiation grafting: Novel mechanisms underlying the interesting enhanced membrane performance. *Sci. Rep.* 2017; **7**, 2721.

[16] S Zinadini, AA Zinatizadeh, M Rahimi, V Vatanpour, H Zangeneh and M Beygzadeh. Novel high flux antifouling nanofiltration membranes for dye removal containing carboxymethyl chitosan coated Fe_3O_4 nanoparticles. *Desalination* 2014; **349**, 145-54.

[17] P Daraei, S Siavash, N Ghaemi, E Salehi, M Ali, R Moradian and B Astinchap. Novel polyethersulfone nanocomposite membrane prepared by PANI/Fe_3O_4 nanoparticles with enhanced performance for Cu(II) removal from water. *J. Membr. Sci.* 2021; **415-416**, 250-9.

[18] X Du, Z Zhang, KH Carlson, J Lee and T Tong. Membrane fouling and reusability in membrane distillation of shale oil and gas produced water: Effects of membrane surface wettability. *J. Membr. Sci.* 2018; **567**, 199-208.

[19] M Farjami, V Vatanpour and A Moghadassi. Fabrication of a new emulsion polyvinyl chloride (EPVC) nanocomposite ultrafiltration membrane modified by para-hydroxybenzoate alumoxane (PHBA) additive to improve permeability and antifouling performance. *Chem. Eng. Res. Des*. 2020; **153**, 8-20.

[20] MB Allabaksh, BK Mandal, MK Kesarla, KS Kumar and PS Reddy. Preparation of stable zero valent iron nanoparticles using different chelating agents. *J. Chem. Pharm. Res.* 2010; **2**, 67-74.

[21] V Piriyawong, V Thongpool, P Asanithi and P Limsuwan. Preparation and characterization of alumina nanoparticles in deionized water using laser ablation technique. *J. Nanomater.* 2012; **2012**, 819403.

[22] ZI Takai, MK Mustafa, S Asman and KA Sekakl. Preparation and characterization of magnetite (Fe_3O_4) nanoparticles by sol-gel method. *Int. J. Nanoelectron. Mater.* 2019; **12**, 37-46.

[23] M Homayoonfal, A Akbari and M Reza. Preparation of polysulfone nanofiltration membranes by UV-assisted grafting polymerization for water softening. *Desalination* 2010; **263**, 217-25.

[24] CS Ong, WJ Lau, PS Goh, BC Ng, T Matsuura and AF Ismail. Effect of PVP molecular weights on the properties of PVDF-TiO_2 composite membrane for oily wastewater treatment process. *Sep. Sci. Tech.* 2014; **49**, 2303-14.

[25] C Mieowkee, P Raoo, YK Eu and JMY Lim. A novel manufacturing process to fabricate double-layer membranes. *Mater. Manuf. Process.* 2016; **31**, 1941-7.
[26] Z Jia and C Tian. Quantitative determination of polyethylene glycol with modified Dragendorff reagent method. *Desalination* 2009; **247**, 423-9.
[27] R Stefanescu, S Brebu, M Matei, I Risca, A Surleva and G Drochioiu. Contribution to casein determination by UV spectrophotometry. *Acta Chem. Iasi* 2017; **25**, 112-26.
[28] AM Rabel, N Raj and B Joseph. Synthesis and characterization of chitosan-coated iron oxide nanoparticles. *In*: Proceedings of the International Conference on Advanced Nanomaterials & Emerging Engineering Technologies, Chennai, India. 2013, p. 6-9.
[29] M Mahdavi, MB Ahmad, J Haron, F Namvar, B Nadi, M Zaki, A Rahman and J Amin. Synthesis, surface modification and characterisation of biocompatible magnetic iron oxide nanoparticles for biomedical applications. *Molecules* 2013; **18**, 7533-48.
[30] K Loh, YH Lee, A Musa, AA Salmah and I Zamri. Use of Fe_3O_4 nanoparticles for enhancement of biosensor response to the herbicide 2,4-dichlorophenoxyacetic acid. *Sensors* 2008; **8**, 5775-91.
[31] F Zamani and S Mohsen. Palladium nanoparticles supported on Fe_3O_4/ amino acid nanocomposite: Highly active magnetic catalyst for solvent-free aerobic oxidation of alcohols. *Catal. Comm.* 2014; **43**, 164-8.
[32] X Huang, W Wang, Y Liu, H Wang, Z Zhang, W Fan and L Li. Treatment of oily waste water by PVP grafted PVDF ultrafiltration membranes. *Chem. Eng. J.* 2015; **273**, 421-9.
[33] Q Chen, Z Yu, Y Pan, G Zeng, H Shi, X Yang, F Li, S Yang and Y He. Enhancing the photocatalytic and antibacterial property of polyvinylidene fluoride membrane by blending Ag-TiO_2 nanocomposites. *J. Mater. Sci. Mater. Electron.* 2017; **28**, 3865-74.
[34] A Qin, X Li, X Zhao, D Liu and C He. Engineering highly hydrophilic PVDF membrane via binding TiO2 nanoparticles and PVA layer onto membrane surface. *Appl. Mater. Interfaces* 2015; **7**, 8427-36.
[35] F Liu, MRM Abed and K Li. Preparation and characterization of poly (vinylidene fluoride) (PVDF) based ultrafiltration membranes using nano γ-Al_2O_3. *J. Membr. Sci*. 2011; **366**, 97-103.
[36] S Harstad, ND Souza, N Soin, AA El-gendy, S Gupta, VK Pecharsky, T Shah, E Siores and RL Hadimani. Enhancement of β-phase in PVDF films embedded with ferromagnetic Gd_5Si_4 nanoparticles for piezoelectric energy harvesting. *AIP Adv.* 2017; **7**, 056411.
[37] J Xiong, Y Gong, C Ma, X Zuo and J He. Fabrication and characterization of polyvinylidene fluoride / zinc oxide membranes with antibacterial property. *J. Water Supply Res. Tech. Aqua* 2020; **69**, 122-33.
[38] J Liu, X Lu and C Wu. Effect of preparation methods on crystallization behavior and tensile strength of poly(vinylidene fluoride). *Membranes* 2013, **3**, 389-405.
[39] MM Ba-abbad, A Wahab, MS Takriff, R Rohania, E Mahmoudia, KA Faneera and A Benamo. Synthesis of iron oxide nanoparticles to enhance polysulfone ultrafiltration membrane performance for salt rejection. 2017; **56**, 1699-704.
[40] G Mago, DM Kalyon and FT Fisher. Membranes of polyvinylidene fluoride and PVDF nanocomposites with carbon nanotubes via immersion precipitation. *J. Nanomater.* 2008; **2008**, 759825.
[41] CM Kee and A Idris. Permeability performance of different molecular weight cellulose acetate hemodialysis membrane. *Separ. Purif. Tech.* 2010; **75**, 102-13.
[42] M Chan and S Ng. Effect of membrane properties on contact angle effect of membrane properties on contact angle. *AIP Conf. Proceed.* 2018; **2016**, 020035.
[43] YH Tan, PS Goh, AF Ismail, BC Ng and GS Lai. Decolourization of aerobically treated palm oil mill effluent (AT-POME) using polyvinylidene fluoride (PVDF) ultrafiltration membrane incorporated with coupled zinc-iron oxide nanoparticles. *Chem. Eng. J.* 2017; **308**, 359-69.
[44] E Akhondi, F Zamani, AWK Law, WB Krantz, AG Fane and JW Chew. Influence of backwashing on the pore size of hollow fiber ultrafiltration membranes. *J. Membr. Sci.* 2017; **521**, 33-42.
[45] L Zheng, WE Price and LD Nghiem. Effects of fouling on separation performance by forward osmosis: The role of specific organic foulants. *Environ. Sci. Pollut. Res.* 2019; **26**, 33758-69.
[46] H Farrajia, NQ Zamana, SKM Sa'at and AF Dashti. Phytoremediation of suspended solids and turbidity of palm oil mill effluent (POME) by Ipomea aquatic. *Eng. Herit. J.* 2017; **1**, 36-40.
[47] T Khanam, WNSW Ata and A Rashedi. Particle size measurement in waste water influent and effluent using particle size analyzer and quantitative image analysis technique. *Adv. Mater. Res.* 2016; **1133**, 571-5.

[48] F Anwar and G Arthanareeswaran. Silver nano-particle coated hydroxyapatite nano-composite membrane for the treatment of palm oil mill effluent. *J. Water Process Eng.* 2019; **31**, 100844.
[49] SM Hosseini, M Afshari, AR Fazlali, SK Farahani, S Bandehali, BVD Bruggen and E Bagheripour. Chemical engineering research and design mixed matrix PES-based nanofiltration membrane decorated by (Fe_3O_4-polyvinylpyrrolidone) composite nanoparticles with intensified antifouling and separation characteristics. *Chem. Eng. Res. Des.* 2019; **147**, 390-8.
[50] Z Rahimi, AA Zinatizadeh and S Zinadini. Membrane bioreactors troubleshooting through preparation of a high antifouling PVDF ultrafiltration mixed matrix membrane nanoparticles. *Environ. Tech.* 2019; **40**, 3523-33.
[51] V Vatanpour, S Shahsavarifar, S Khorshisi and M Masteri-Farahani. A novel antifouling ultrafiltration membranes prepared from percarboxylic acid functionalized SiO_2 bound Fe_3O_4 nanoparticle (SCMNP-COOOH)/polyethersulfone nanocomposite for BSA separation and dye removal. *J. Chem. Tech. Biotechnol.* 2019; **94**, 1341-53.
[52] J Sun, S Li, Z Ran and Y Xiang. Preparation of Fe_3O_4@TiO_2 blended PVDF membrane by magnetic coagulation bath and its permeability and pollution resistance. *J. Mater. Res. Tech.* 2020; **9**, 4951-67.
[53] WQ Ng, SO Lai, KC Chong, SS Lee, CH Koo and WC Chong. Reduction of total suspended solids, turbidity and colour of palm oil mill effluent using hybrid coagulation-fltrafiltration process. *J. Appl. Membr. Sci. Tech.* 2018; **23**, 73-88.
[54] M Said, AW Mohammad, MTM Nor, SRS Abdullah and HA Hasan. Investigation of three pre-treatment methods prior to nanofiltration membrane for palm oil mill effluent treatment. Sains Malaysiana 2015; **44**, 421-7.